Molecular Crystals and Liquid Crystals

Publication details, including instructions for authors and subscription information:
http://www.tandfonline.com/loi/gmcl20

Physical Properties of Metastable Nanocrystalline Sm-Fe-Si Alloys

A. Nandra* [a], E. Burzo [a], L. Bessais [b], C. Djega-Mariadassou [b] & V. Lalanne [b]

[a] Faculty of Physics, Babes-Bolyai University, Romania

[b] LCMTR, UPR 209, CNRS, Thiais, France

Version of record first published: 18 Oct 2010

To cite this article: A. Nandra*, E. Burzo, L. Bessais, C. Djega-Mariadassou & V. Lalanne (2004): Physical Properties of Metastable Nanocrystalline Sm-Fe-Si Alloys, Molecular Crystals and Liquid Crystals, 417:1, 47-55

To link to this article: http://dx.doi.org/10.1080/15421400490478777

Mol. Cryst. Liq. Cryst., Vol. 417, pp. 47/[531]–55/[539], 2004

ISSN: 1542-1406 print/1563-5287 online
DOI: 10.1080/15421400490478777

Taylor & Francis
Taylor & Francis Group

PHYSICAL PROPERTIES OF METASTABLE NANOCRYSTALLINE Sm-Fe-Si ALLOYS

A. Nandra and E. Burzo*
Babes-Bolyai University, Faculty of Physics,
3400 Cluj-Napoca, Romania

L. Bessais, C. Djega-Mariadassou, and V. Lalanne
LCMTR, UPR 209, CNRS,Thiais, France

The presence of nanocrystalline $SmFe_{9-x}Si_x$ ($x \leq 1$) phase, has been evidenced in Sm-Fe-Si system. This crystallizes in a hexagonal structure having P6/mmm space group. The X-ray analyses show that silicon is located in 3g sites. The ^{57}Fe Mősbauer spectra were decomposed in 8 sextets corresponding to 2e, 3g and 6l sites with different local environments. The mean hyperfine field values follow the sequence $B_{HF}(2e) > B_{HF}(6l) > B_{HF}(3g)$.

Keywords: metastable phase; Mössbauer spectroscopy; Sm-Fe-Si alloys

I. INTRODUCTION

The R_2Fe_{17} series of compounds where R is rare earth, are notable from their low Curie temperatures, T_c [1]. The highest T_c value in the series ($T_c \cong 477$ K) obtained for Gd_2Fe_{17} compound is still about 600 K lower than the T_c value of α-Fe. In order to improve the properties of R_2Fe_{17} compounds, particularly Sm_2Fe_{17}, for their use in technical applications, substitutions at iron sites were performed. As example, the particular substitution of Ga, Al or Si for Fe into Sm_2Fe_{17} stabilizes the crystal structure and increases the Curie temperature [2]. A considerable increase of the Curie temperature can be achieved also by alloying with carbon or nitrogen.

The metastable phases in the Sm-Fe system close to composition 2:17 are of technical interest. The metastable $TbCu_7$ – type structure was previously reported [3]. This structure can be derived from the $CaCu_5$ one,

*Corresponding author. Tel.: +40 264 194315, Fax: +40 264 191906, E-mail: anandra@phys.ubbcluj.ro

in which RM_5 compounds (M = Co, Ni) crystallize. The iron does not form compounds of this series, but nonstoichiometric $R_{1-s}M_{5+2s}$ phases still exist. For s = 0.22 the $TbCu_7$ phase is formed. When s = 0.33, the stoichiometric R_2M_{17} compounds can be obtained. In $TbCu_7$ type structure the 3g sites characteristic for RM_5-type structure still exist, but 2c sites are splitted in (*1−3s*) 2c and (*s*) 6l sites [4].

In the present paper we analyze the metastable phases in Sm-Fe-Si system. In addition to $TbCu_7$ type structure, we evidence a new metastable phase, with s = 0.35–0.36 having composition close to $SmFe_9$ [5].

II. EXPERIMENTAL METHODS

The $SmFe_{9-x}Si_x$ samples, with x = 0.25, 0.5, 0.75 and 1.0, were prepared by the high-energy ball milling and subsequent annealing. Mechanical milling is particularly suitable for obtaining nanocrystalline reactive powders. By this method a better control of the overall stoichiometry than by conventional melting method can be obtained. The powders were milled during 5 hours in a high-energy planetary ball mill. The as-milled powders were wrapped in tantalum foils and annealed in a silica tube at 973 K during 30 min.

The X-ray patterns were recorded by means of a Bruker diffractometer mounted with Bragg-Brentano geometry and an automatic divergence slit, using Cu K_α radiation. The data treatment was carried out by a Rietveld refinement using the FULLPROF computer code. Scanning electron microscopy (SEM) with X-ray microanalysis facilities were performed on a Jeol-JSM 5600 LV microscope equipped with an EDX spectrometer. In addition, High-Resolution Transmission Electron Microscopy (HRTEM) analyses were also made.

The ^{57}Fe Mossbauer spectra were collected at room temperature using a constant-acceleration spectrometer, working in the mirror image mode.

III. RESULTS AND DISCUSSIONS

3.1. Crystallographic Study

a. Phase Formation and Structure

The X-ray diffraction (XRD) patterns of the $SmFe_{9-x}Si_x$ alloys with $x \leq 1$, annealed at 973 K, are shown in Figure 1. The main phases are hexagonal having P6/mmm type structure. In addition small quantities of iron were observed for sample with $x \geq 0.5$. The presence of free iron suggests that the annealing temperature was too small for the formation of only 1/9 phase. A small amount of Sm_2O_3 was also observed. This may be due to oxygen traces, still present in the initial powders. (Fig. 1)

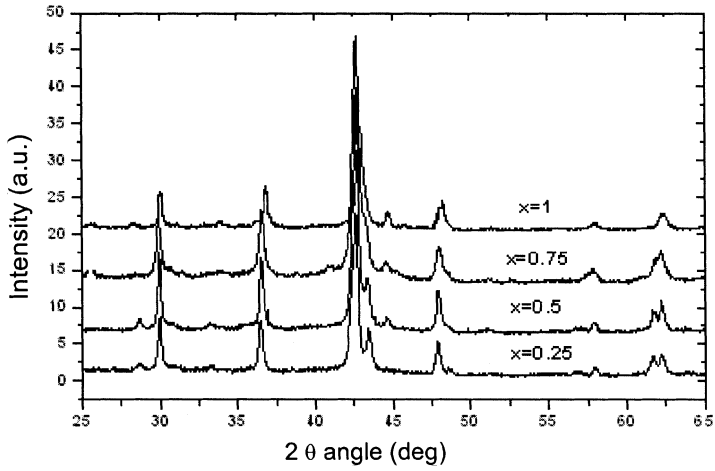

FIGURE 1 X-ray diffraction patterns of $SmFe_{9-x}Si_x$ alloys with $x \leq 1$, annealed at 973 K.

The lattice parameters determined for $SmFe_{9-x}Si_x$ alloys with $x \leq 1$, are presented in Table 1. The Rietveld refinements have been performed. (Fig. 2). These suggest that Si is located in *3g* sites. The *a* cell parameters are found to decrease while the *c* ones increase, particularly above $x = 0.5$. A simple steric effect of Fe substitution ($r_{Fe} = 1.26$ Å) by smaller Si atom ($r_{Si} = 1.17$ Å) may explain such behavior for composition dependence of a lattice constant. Above $x = 0.5$, some additional Sm atoms are substituted for Fe-Fe dumbbells, thus increasing the c parameters [3]. (Table 1)

TABLE 1 The Lattice Parameters, *a* and *c*; *D* Mean Diffraction Domaine Size; R_B and X_2 the Classical Goodness-of-fit Parameters, *x, z* Axe Coordinates for 6*l* to 2*e* Sites

	X = 0.25	X = 0.50	X = 0.75	X = 1.00
s	0.35	0.35	0.35	0.36
a (Å)	4.921	4.917	4.904	4.889
c (Å)	4.163	4.159	4.172	4.184
D (nm)	26.5	25.5	23.5	21.6
R_B	5.48	6.37	5.80	5.88
X_2	1.69	1.39	1.87	1.56
X(6l)	0.291	0.291	0.289	0.291
Z(2e)	0.289	0.290	0.290	0.289

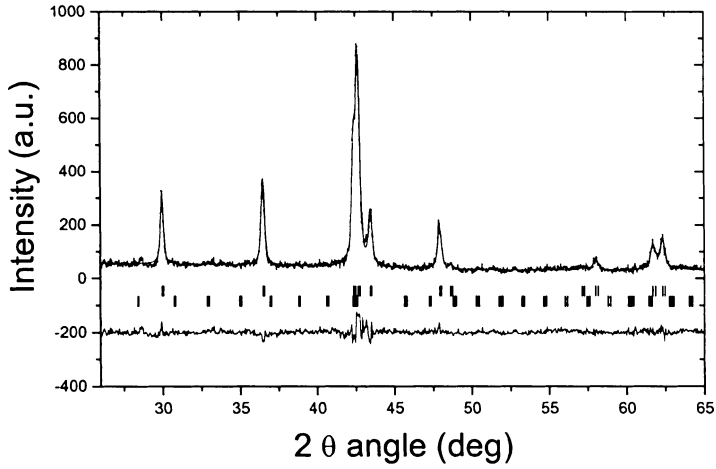

FIGURE 2 Rietveld analysis of $SmFe_{9-x}Si_x$ ($x = 0.25$) annealed at 973 K.

The Wigner-Seitz cell (WSC) volumes have been calculated by means of Dirichlet domains and are presented in Figure 3 as function of Si content. We computed also the local environments for various iron sites. The numbers of nearest neighbor atoms as well as the distance between them, obtained in case of $SmFe_8Si$ are listed in Table 2.

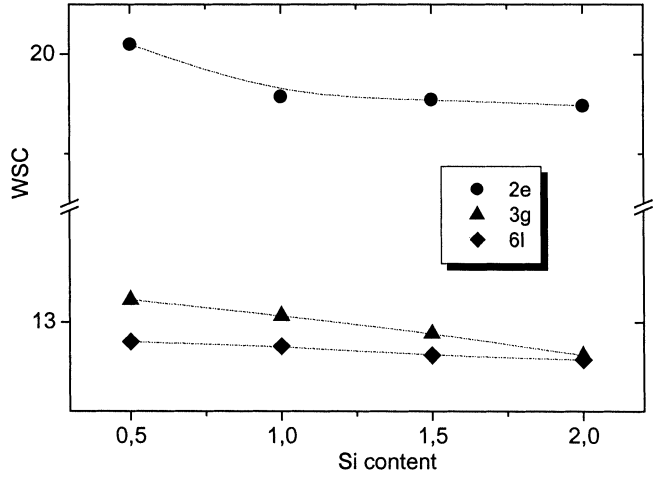

FIGURE 3 Wigner-Seitz volume versus silicon content of $SmFe_{9-x}Si_x$ alloys with $x \leq 1$.

TABLE 2 The Interatomic Distance of Hexagonal P6/mmm Structure for $SmFe_8Si$ Compound

		Fe(2e)		Fe(61)		Fe(3g)/Si		
x	Site	Number distance of Fe atoms (Å)		Number distance of Fe atoms (Å)		Number distance of Fe atoms (Å)		Iron near neighbors
	Fe (2e)	1	2.41	6	2.75	6	2.60	12.36
0.50	Fe (6l)	2	2.74	2	2.46	6	2.45	9.36
	Fe (3g)/Si	2	2.60	4	2.45	4	2.44	9.57

The WSC volumes resulting from such calculation follow the volume sequence: $V\{2e\} > V\{3g\} > V\{6l\}$. This sequence is not dependent on the Si content. (Fig. 3)

b. Electron Microscopy (SEM and HRTM)

SEM micrographs obtained in case of $SmFe_8Si$ alloy are plotted in Figure 4a. The particles dimensions are around 1 μm (Fig. 4b) and form uniform agglomerates with sizes smaller than 10 μm. The X-ray microanalyses performed on the selected areas, on the same alloy, are shown in Figure 5. There are homogenous distributions of Sm, Fe and Si in all sample. Similar

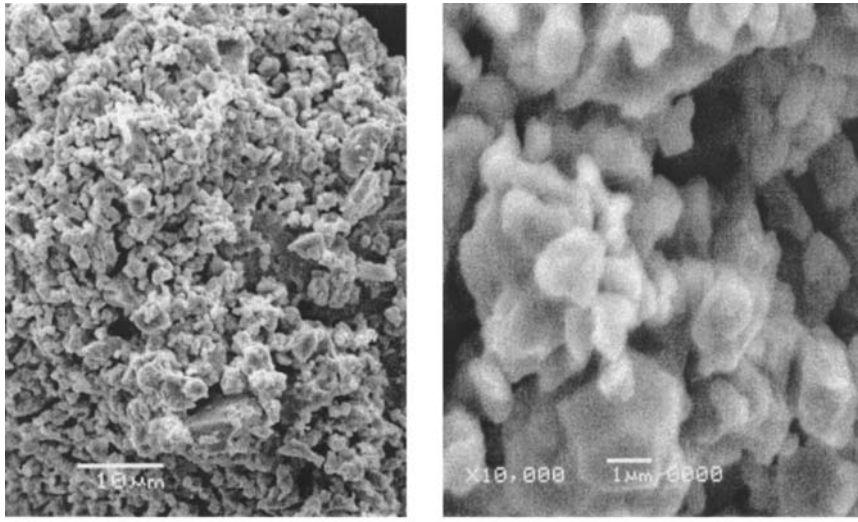

FIGURE 4 SEM micrographs for $SmFe_8Si$ sample.

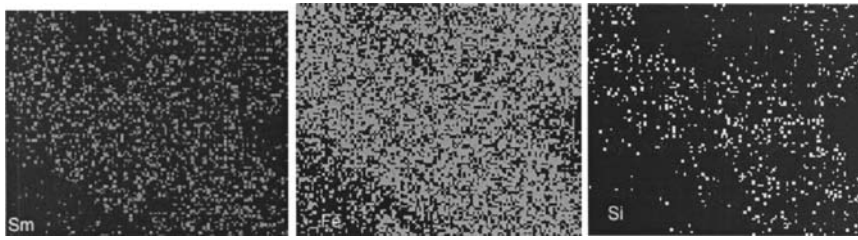

FIGURE 5 The maps of Sm, Fe and Si distributions of $SmFe_{8.5}Si_{0.5}$ compound.

results were obtained also for other compositions. The chemical analyses show 4.27 at % Si content 84 at % Fe content and 12 at % Sm content. This result confirms the initial composition of the starting powder.

Figure 6 shows a high resolution HRTEM lattice image of the $SmFe_{8.5}Si_{0.5}$ sample. The sizes of crystallites are in the range of 20–25 nm in agreement with XRD investigation on the same sample.

c. Mossbauer Effect Studies

The ^{57}Fe Mossbauer spectra of $SmFe_{9-x}Si_x$ alloys with $x \leq 1$, at room temperature, are plotted in Figure 7. The analyses of the spectra were performed based upon two criteria: (1) the contributions of various sites were distinguished by their relative intensities and local environment effects and (2), the correlation of the hyperfine parameters of the crystallographic sites with to their Wigner-Seitz cell (WSC) volumes. The larger the Wigner-Seitz volume, the higher isomer shift is expected.

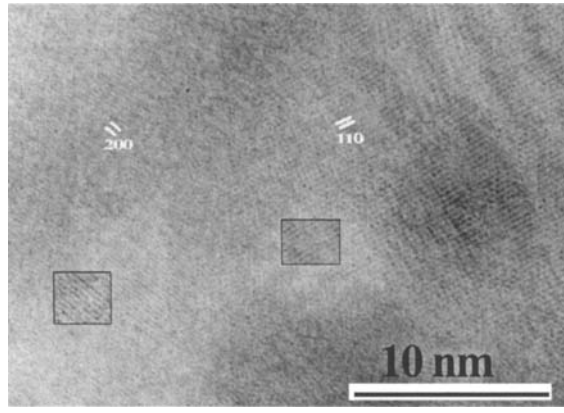

FIGURE 6 HRTM lattice image for $SmFe_{8.5}Si_{0.5}$ alloys.

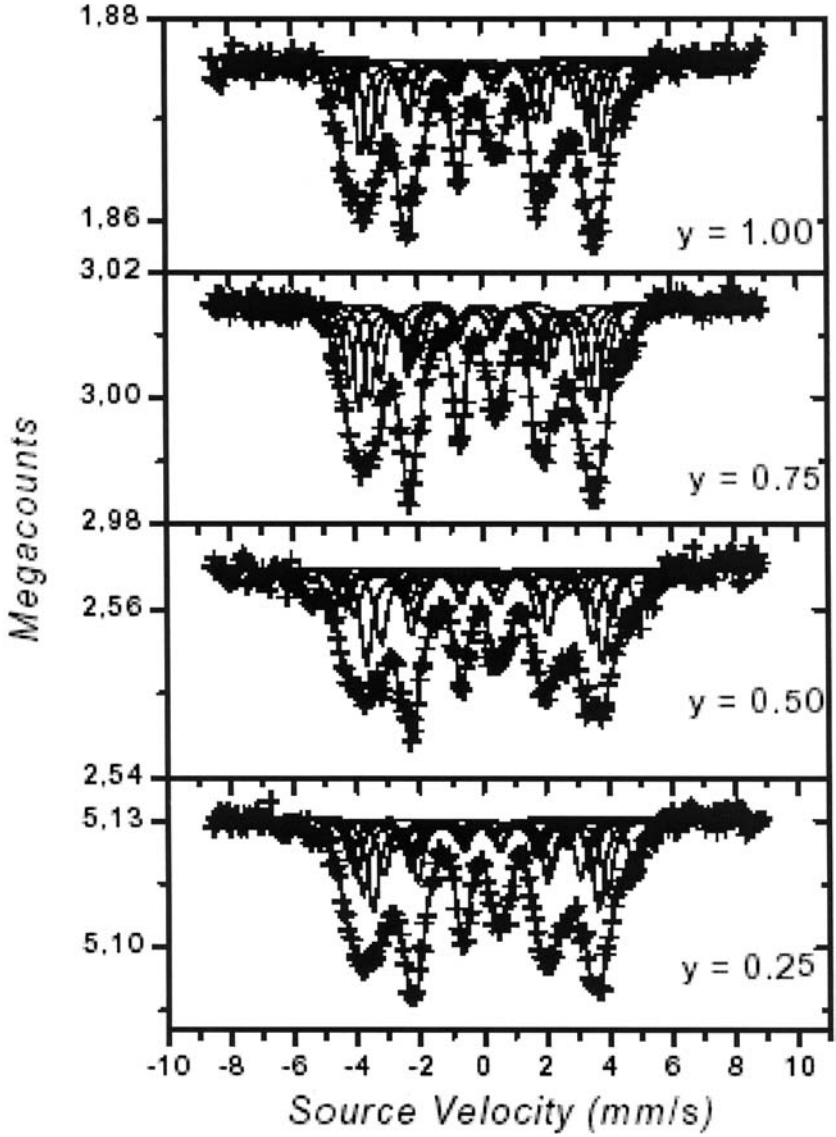

FIGURE 7 The Mossbauer spectra of $SmFe_{9-x}Si_x$ alloys with $x \leq 1$, at 293 K.

Based on the above supposition the spectra were decomposed in 8 sextets corresponding to 2e, 3g and 6l sites in the different local environments. Thus, two sextets were evidenced for 2*c* sites, three for 3*g* and three for *6*l. The isomer shift and hyperfine field evolutions versus Si content, at room

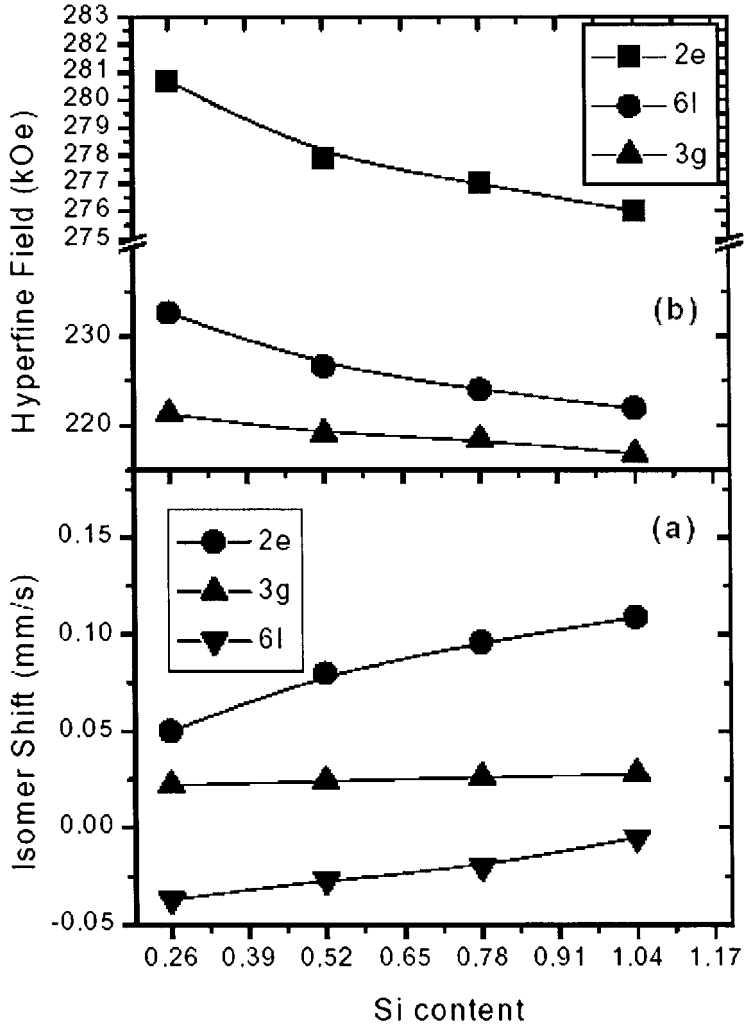

FIGURE 8 The isomer shifts (a) and the hyperfine fields (b) for $SmFe_{9-x}Si_x$, $x \leq 1$ alloys.

temperature for the different sites, are presented in Figure 6a, and Figure 6b, respectively. We note that the increase of the mean isomer shift of the 2*e* and 6*l* atoms upon silicon substitution is an agreement with WSC volumes.

For the 3g iron sites the isomer shift remains nearly constant. This result can be understood in terms of the preferential silicon occupation. The 2*e*

and 6*l* iron sites have six adjacent 3g neighbors while the 3g sites have only four 3g neighbors. The 3g-sites with the smaller number of 3g neighbors are the least affected by the silicon substitution and their charge density at the nucleus is not modified.

The ^{57}Fe hyperfine fields are dominated by two contributions: a negative core electron (1s, 2s, 3s) polarization field H_{CE}, produced by 3d electrons via exchange interaction, and a positive field H_{4s} produced from self-polarization of 4*s* conduction electrons. As result of this competition the following sequence of the hyperfine field results B_{HF} (2e) > B_{HF} (6l) > B_{HF} (3g) for all compounds. The mean hyperfine fields decrease with increasing Si content. This fact may be attributed to 3d-2p hybridization effects.

III. CONCLUSIONS

The presence of new metastable phase 1/9 was evidenced in Sm-Fe-Si system. This correspond to composition $Sm_{1-s}Fe_{5+2s}$ with s = 0.36–0.38. This phase, as 1/7 one previously reported, can be considered as a possible precursor for the 2:17 rhombohedral type structure. In 1/9 phase the silicon is preferentially located in 3g sites. The a lattice parameters decrease while c increase when substituting iron by silicon. The contraction along a direction can be related to smaller silicon radius than that of iron while the increase along c to the presence of dum-bell sites. The Mossbauer spectra were decomposed according the sites occupied by iron as well as their dominant local environments. The isomer shifts are close related to WSC volume. The decrease of the ^{57}Fe hyperfine field when increasing silicon content can be correlated with hybridization effects.

REFERENCES

[1] Burzo, E., Chelkovski, A., & Kirchmayr, H. R. (1990). In: Landold-Borstein Handbuch, Springer Verlag: Berlin, Vol. 19d3.
[2] Handstein, A., Kubis, M., Cao, L., Gebel, B., & Muller, K. H. (1999). *J. Magn. Magn. Mater.*, *192*, 281.
[3] Buschow, K. H. J. & der Goot, A. S. V. (1968). *J. Less-Common. Met.*, *14*, 323.
[4] Givord, D., Laforest, J., Schweizer, J., & Tasset, F. (1979). *J. Appl. Phys.*, *50*, 2008.
[5] Djega-Mariadassou, C. & Bessais, L. (2000). *J. Magn. Magn. Mater.*, *210*, 81.